Case Studies in Construction Materials 23 (2025) e05336

Contents lists available at ScienceDirect

Case Studies in Construction Materials

journal homepage: www.elsevier.com/locate/cscm

Effect of mono-ethylene glycol on hydration and mechanical properties of waste glass replacement cement composites

Hyunuk Kang [a], Jian-Xin Lu [b], Jingwei Yang [a], Ahyeon Lim [a], Namgyu Park [a], Juhyuk Moon [a,c,*], Chi Sun Poon [b]

[a] Department of Civil and Environmental Engineering, Seoul National University, Seoul 08826, Republic of Korea
[b] Department of Civil and Environmental Engineering, and Research Centre for Resources Engineering towards Carbon Neutrality, The Hong Kong Polytechnic University, Hong Kong, China
[c] Institute of Construction and Environmental Engineering, Seoul 08826, Republic of Korea

ARTICLE INFO

Keywords:
Sustainable cement
Waste glass
Mono-ethylene glycol
Hydration mechanism, grindability

ABSTRACT

The increasing demand for sustainable construction materials has highlighted the need to utilize industrial by-products as supplementary cementitious materials (SCM). In particular, waste glass (WG) has attracted attention due to its abundance. However, its low reactivity and large particle size limit practical applications in cementitious systems. To address this limitation, this study investigates the feasibility of using mono-ethylene glycol (MEG) as a grinding agent to enhance both the ordinary Portland cement (OPC) and pozzolanic reactivities of WG. The research focuses on improving the hydration performance and mechanical properties of WG-substituted OPC composites while simultaneously promoting resource recycling and reducing CO_2 emissions. Experimental results demonstrate that MEG induces subtle modifications in the hydration behavior of OPC and significantly increases the pozzolanic activity of WG, leading to greater calcium silicate hydrate formation and pore structure refinement. Remarkably, the incorporation of only 0.05 % MEG achieved superior compressive strength at both 1 and 28 days compared to 100 % OPC samples. These findings suggest that the proposed approach provides an efficient and eco-friendly strategy for enhancing WG recycling rates and lowering the embodied CO_2 emissions of cement-based materials.

1. Introduction

Ordinary Portland cement (OPC) is one of the most widely used materials globally. Its popularity stems from its excellent cost-effectiveness and outstanding mechanical properties [1–3]. However, OPC production is associated with the emission of a substantial amount of CO_2 due to the high-temperature calcining process, rendering it an unsustainable structural material from an environmental perspective [4,5]. This conflicts with the goals of achieving carbon neutrality by 2050, underscoring the urgent need to develop alternative construction materials [2,6,7]. Various strategies have been proposed to address this issue, with one of the most prominent being the use of supplementary cementitious materials (SCMs), such as ground-granulated blast-furnace slag and fly ash [8–15]. However, these by-products have been extensively utilized as SCMs for decades and are increasingly applied in other industries, driving their prices steadily upward [16,17].

* Corresponding author at: Department of Civil and Environmental Engineering, Seoul National University, Seoul 08826, Republic of Korea
E-mail address: juhyukmoon@snu.ac.kr (J. Moon).

https://doi.org/10.1016/j.cscm.2025.e05336
Received 14 June 2025; Received in revised form 24 August 2025; Accepted 19 September 2025
Available online 20 September 2025

An alternative approach to reduce OPC consumption involves converting underutilized by-products into SCMs. Recently, there has been growing interest in using waste glass (WG) as a construction material [18–21]. Glass is widely produced across various sectors due to its versatility and cost-effectiveness, with an estimated global production of approximately 300 million tons annually [22–24]. However, due to its limited durability, glass often has a short service life, leading to substantial amounts of WG being discharged [25,26]. WG encompasses various types, including soda-lime glass, crystal glass, borosilicate glass, and electric glass [25]. The differing melting temperatures among these glass types complicate their recycling process [27]. Furthermore, even trace amounts of non-recyclable WG (as low as ~0.0005 wt%) can render the entire batch unsuitable for recycling. Therefore, developing effective technologies to repurpose WG is imperative.

WG has been explored for use in various construction materials. One of the earliest approaches involved utilizing WG as aggregate, and numerous studies have reported on its applications [28–30]. However, the widespread use of WG as aggregate has been limited due to challenges associated with alkali-silica reaction (ASR) [31–33]. Furthermore, other researchers have introduced methods for using WG as SCMs through further grinding [34–37]. That is, although various types of WG-containing SCMs have been utilized to develop eco-friendly blended cements, fundamental studies on their hydration mechanisms remain very limited. As expected, given that WG contains a significant amount of amorphous SiO_2, it has the potential to participate in pozzolanic reactions with $Ca(OH)_2$. Amorphous SiO_2 is reported to exhibit high pozzolanic reactivity due to its long-chain structure and randomly arranged atoms, which provide a relatively large number of reactive sites [38]. Moreover, it has been reported that WG can mitigate ASR [27,39,40]. While studies have investigated the reactivity of WG based on its grindability [41–43], research on the mechanochemical effects of GA on WG has been very limited. This gap highlights the need for further exploration in this area.

GAs are organic solution typically introduced during the fine grinding of cementitious materials [10,44–48]. Due to their appropriate viscosity and torque, GAs effectively transfer the external energy generated by ball mills to the powder, thereby improving grindability [46,49,50]. Commonly used GAs include alkanolamine-based solutions such as triethanolamine (TEA), triisopropanolamine (TIPA), ethanol diisopropanolamine (EDIPA), and diethanol isopropanolamine (DEIPA) [49,51–54]. These alkanolamine-based solutions are known to significantly enhance aluminate reactions (i.e., C_3A and C_4AF phases). In addition to alkanolamine-based GAs, glycol-based GAs are also utilized for cementitious materials [55,56]. Examples include mono-ethylene glycol (MEG) and diethylene glycol, which have been deeply studied [57]. Furthermore, a study suggests that glycol-based GAs play a more favorable role in improving grindability compared to alkanolamine-based GAs [58]. These glycol-based solutions are reported to partially modify the crystal structure of calcium silicate hydrate (C-S-H), leading to enhanced mechanical properties [59,60].

Based on the aforementioned phenomena, it is hypothesized that using the most cost-effective glycol, MEG, as a GA could not only enhance the reactivity of the amorphous SiO_2 present in WG but also improve the strength of C-S-H. This, in turn, could significantly improve the mechanical properties of WG-substituted OPC (WG-OPC). Accordingly, this study investigates the mechanochemical effects of WG-OPC using four different dosages of MEG as a GA. Firstly, the impact of MEG on the grindability of WG was evaluated through particle size distribution analysis. To examine the effects of MEG on the hydration properties of WG-OPC, techniques such as isothermal calorimetry, thermogravimetric analysis (TGA), and X-ray diffraction (XRD) were employed. In particular, the partial or no crystalline structure (PONKCS) method was utilized to analyze the phase assemblage of amorphous C-S-H and WG, respectively. Furthermore, micro-computed tomography (μ-CT) was used to evaluate the porosity characteristics of WG-OPC influenced by MEG. This study presents a novel approach to activating WG through the combined use of mechanical grinding and MEG, which serves as a GA. While previous efforts have focused primarily on physical size reduction to enhance pozzolanic activity, the proposed method leverages the dual role of MEG in improving grindability and promoting hydration reaction of WG-OPC composite. This integrated strategy allows for more efficient utilization of WG as a SCM and introduces a practical, low-dosage technique for improving the performance of WG-OPC composites.

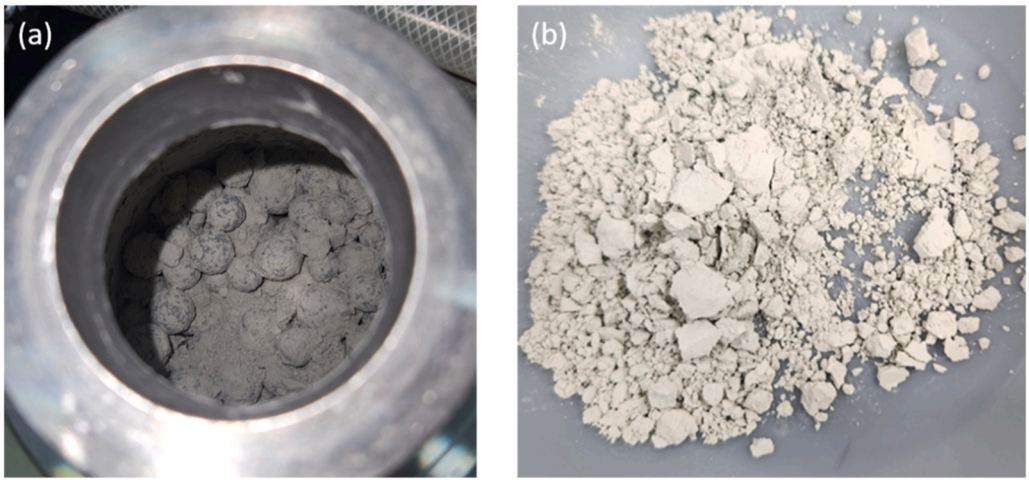

Fig. 1. Agglomeration phenomena among particles of WG powder ground for 10 h.

2. Materials and methods

2.1. Sample preparation

The materials used in this study were Type 1 ordinary Portland cement (OPC) (Hanil Cement Co., Ltd., Seoul, Republic of Korea) and brown glass bottles (i.e., soda-lime glass) with a specific gravity of 2.52 g/cm^3. For WG, coarse-crushed nodules smaller than 4.76 mm were selected and further ground using a Lab Jar Mill QM-5 device (Konenano Co. Ltd., Seoul, Republic of Korea). The grinding conditions involved processing 214 g of WG at 180 rpm for 8 h. These conditions were determined through multiple pretests to optimize the grinding performance of the ball mill and to prevent agglomeration among WG particles (Fig. 1**(a and b) and** Fig. 2). Excessive grinding for 10 h led to agglomeration among WG particles, which could hinder their proper dispersion when replacing OPC in WG-OPC composites. Therefore, the optimal grinding duration was determined to be 8 h. In addition, the same grinding conditions were employed to prepare WG with varying amounts of MEG (i.e., 0, 0.02, 0.05, and 0.1 %). The mineralogical properties of OPC and WG were analyzed using XRD and XRF, and the results are summarized in Tables 1 and 2. Finally, to produce WG-OPC composites, the mix proportions shown in Table 3 were used.

2.2. Experimental method

2.2.1. Specimen preparation process

To evaluate the mechanical properties of the mortar specimens investigated in this study, cubic specimens with dimensions of 50 × 50 × 50 mm^3 were prepared. The curing conditions of the specimens were as follows: After casting the mortar into molds, the specimens were sealed and stored in a controlled chamber at 20 °C and 60 % relative humidity until demolding (i.e., 1 day). After demolding, the specimens were subjected to water curing at 20 °C until the designated compressive strength testing dates. Compressive strength tests were conducted on 1, 2, 7, and 28 days to assess both the early- and late-stage mechanical properties of WG-OPC composites and analyze their pozzolanic reaction. For each curing age, compressive strength measurements were performed on three specimens.

2.2.2. Particle size distribution measurement

The particle size distribution of WG was analyzed using a particle size distribution analyzer (Malvern Instruments Ltd., Malvern, UK). Isopropyl alcohol was used as the dispersing medium to prevent any potential chemical reactions.

2.2.3. ICP-OES measurement

An inductively coupled plasma atomic emission spectrometer (5100 SVDV ICP-OES, Agilent Ltd., CA, USA) was used to analyze the ion dissolution behavior of WGOPC during the early stages of hydration. The water-to-binder ratio of the slurry for analysis was set at 10:1. The slurry was stirred at 20 °C for 30, 60, 120, and 240 min, after which the solution and solid were separated via centrifugation. The solution was then fully extracted using a 200 nm filter [44]. Finally, a magnetic induction field was utilized to generate plasma argon, and the obtained solution was deposited and injected into the particles for analysis [61].

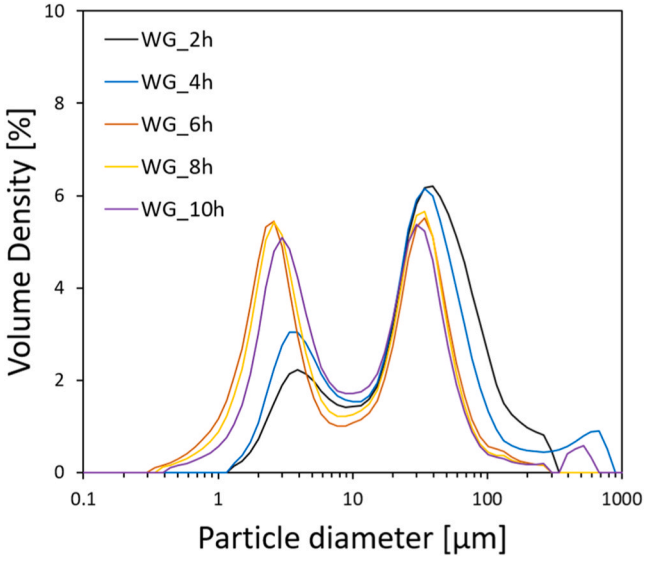

Fig. 2. Effect of grinding time on the particle size distribution of WG.

Table 1
X-ray fluorescence analysis results of OPC and WG.

Phases	OPC (unit %)	WG (unit %)
CaO	62.6	9.5
SiO_2	19.7	68.1
Al_2O_3	5.0	2.8
Fe_2O_3	3.6	1.2
MgO	2.8	1.7
SO_3	2.8	0.1
K_2O	0.9	0.9
P_2O_5	0.3	-
TiO_2	0.3	0.1
ZnO	0.1	-
MnO	0.1	-
SrO	0.1	0.1
Na_2O	-	14.6
BaO	-	0.3
Pd	0.1	-
Cr_2O_3	-	0.2
LOI	1.8	0.4

Table 2
QXRD analysis results of OPC and WG powder.

Phase	OPC	WG
C_3S (M3)	42.4	-
C_2S (beta)	26.0	-
C_3A (cubic)	2.9	-
C_3A (orthorhombic)	1.3	-
C_4AF	11.4	-
Calcium carbonate	7.9	-
Gypsum	4.1	-
Periclase	2.9	-
Dolomite	1.1	-
Mullite	-	-
Quartz	-	-
Amorphous	-	100

Table 3
Mix proportions of WG-OPC composites.

Sample label	OPC (g)	WG (g)	Aggregate (g)	MEG* (g)	Water (g)
O100	450	-	1350	-	225
WG-OPC−0 %	337.5	112.5	1350	-	225
WG-OPC−0.02 %	337.5	112.5	1350	0.0225	225
WG-OPC−0.05 %	337.5	112.5	1350	0.0563	225
WG-OPC−0.1 %	337.5	112.5	1350	0.1125	225

* Added before grinding WG

2.2.4. Isothermal calorimeter measurement

To analyze the effect of MEG on the early hydration behavior of WG-OPC, an 8-channel calorimeter (TA Instruments, New Castle, DE, USA) was utilized. To maintain consistency with the mix proportions used for compressive strength measurements, paste with a water-to-binder ratio of 0.5 was prepared for the analysis. A total of 15 g of slurry was uniformly mixed for 2 min, and 6 g of the slurry was then placed into the calorimeter. Finally, the obtained data were corrected using the specific heat of the materials included in the mixture.

2.2.5. Hydration stop method

To achieve precise analysis of the hydration reactions of WG-OPC, an optimized pretreatment process was applied. That is, a hydration stoppage method was employed to remove free water from the paste powder. First, the paste specimens were finely ground for 5 min, during which a specific amount of isopropyl alcohol was added to prevent rapid temperature increases. The ground paste powder samples were then immersed in isopropyl alcohol for 20 min to completely replace the free water in the paste with isopropyl alcohol. Subsequently, the samples were immersed in diethyl ether for 5 min to replace the isopropyl alcohol with diethyl ether. A vacuum pump was used to remove visible diethyl ether, and the remaining diethyl ether in the powder was evaporated entirely by

storing the samples in a chamber set at 40 °C for 15 min [62,63].

2.2.6. TGA measurement

To analyze the hydration properties of WG-OPC in this study, an SDT Q600 differential scanning calorimeter (DSC)-TG system (TA Instruments Ltd., Newcastle, DE, USA) was employed. A platinum holder with excellent thermal conductivity was used to precisely analyze the thermal decomposition of minerals. During the measurement process, N_2 gas was introduced at a flow rate of 100 mL/min to prevent potential carbonation effects. Furthermore, standard conditions widely used for analyzing the hydration of cementitious materials were applied: a heating rate of 10 K/min and a temperature range from ambient temperature to 1000 °C [62].

2.2.7. Method for XRD measurement and analysis

The XRD patterns were measured using a D2 Phaser X-ray diffractometer (Bruker Co. Ltd., Land Baden-Württemberg, Germany), equipped with a Cu Kα radiation source. The instrument operated at a voltage of 30 kV and a current of 10 mA, providing optimal conditions for analyzing the mineralogical properties of cementitious materials [64,65]. TOPAS software version 7.0 (Bruker Co. Ltd., Land Baden-Württemberg, Germany) was utilized for the analysis of the XRD patterns. For qualitative phase analysis, the crystallography open database was employed. In addition, quantitative phase analysis was conducted following these procedures: first, the background of the patterns was modeled using a 0th or 1st-order Chebyshev polynomial with the inclusion of a 1/X term. Rietveld refinement for each mineral phase was carefully performed, adhering to methods established in previous studies [66,67].

In this study, the PONKCS method was used to quantitatively evaluate the amorphous C-S-H and WG (Fig. 3**(a and b)**). For WG, no crystalline phases were detected, and only an amorphous hump was observed. To create the PONKCS model for WG phase, 2 g of an internal standard material (Al_2O_3) and 2 g of WG powder were mixed for 30 min, and the XRD pattern was measured. The obtained XRD pattern was then used to calculate/simulate the virtual scale factor, Miller indices, and cell volume of WG based on the known weight ratio. The PONKCS model for the amorphous C-S-H was developed using the XRD pattern of OPC hydrated for 7 years, as reported in a previous studies [68,69]. Furthermore, the model was constructed using the space group F2dd that best represents the C-S-H [70]. To correct the quantities of minerals calculated using the aforementioned procedure, the weight loss value at 600 °C, i.e., chemically bound water (CBW), was used. That is, CBW contained within the hydration products formed through the reaction between water and minerals was utilized for this correction [10,44,46,62].

2.2.8. Method for micro-CT measurement and analysis

High-resolution micro-CT imaging (Skyscan 1272, Bruker, Kontich, Belgium) was utilized to acquire 1800 projection images with a rotation increment of 0.3° and an exposure duration of 6000 ms. The tomographic reconstruction of the data was carried out using NRecon software (Bruker, Kontich, Belgium). For the porosity analysis, a 1 mm cylindrical specimen was selected, focusing on pores with diameters of 3 μm or greater. Porosity measurements were derived from a central region of the sample measuring $900 \times 1650 \times 2700\ \mu m^3$, with a resolution of 3 μm per pixel. Image segmentation, 3D visualization, and porosity determination were conducted using AVIZO software (Thermo Fisher Scientific, Waltham, MA, USA). To enhance the accuracy of pore segmentation, Gaussian filtering was applied to reduce noise, followed by the implementation of the Otsu thresholding method, which classified pores based on grayscale intensity [71].

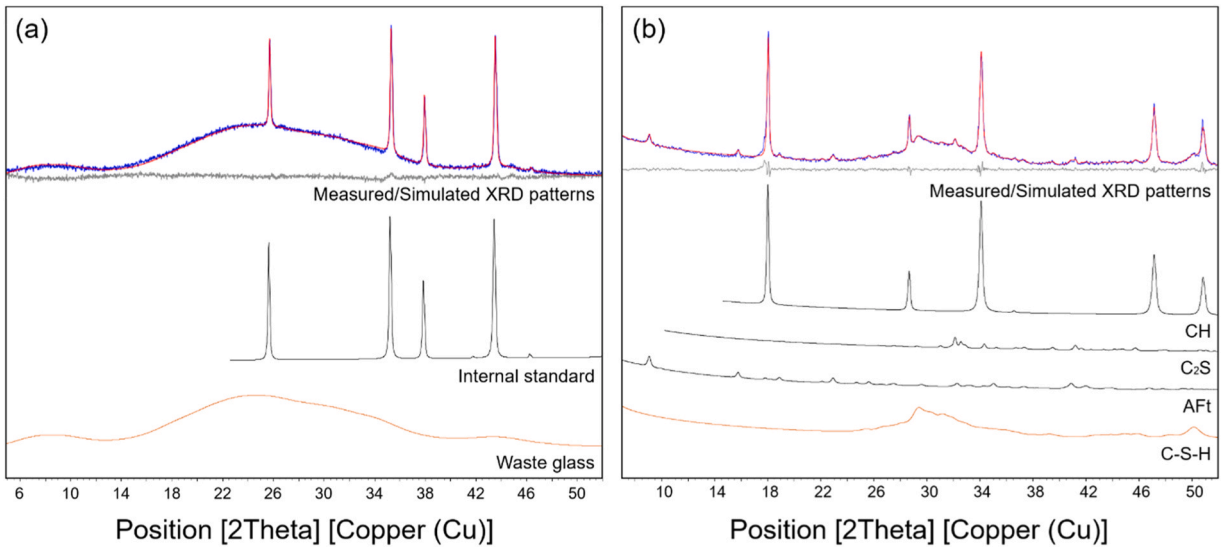

Fig. 3. Simulated diffraction patterns of (a) WG and (b) C-S-H using PONKCS method.

3. Results

3.1. Particle size distribution and specific surface area

Fig. 4**(a)** presents the particle size distributions of WG with varying amounts of MEG added. In all samples, two distinct peaks were observed. With the addition of MEG, the second mode (from 11 to 300 μm) shifted to the left, accompanied by an increase in peak intensity. This trend was evident up to the MEG dosage of 0.05 %, but at 0.1 %, the peak shifted back to the right. In contrast, the first mode (from 0.5 to 8 μm) exhibited a decrease in peak intensity with the addition of MEG. These observed results align with previously reported findings, suggesting that the addition of optimal amounts of GA improves grindability of cementitious materials, while excessive amounts can adversely affect grinding performance [49,72]. Furthermore, Fig. 4**(b)** presents the specific surface area results. Similar to the particle size distribution findings, the specific surface area increased with the addition of MEG up to a dosage of 0.05 %. However, at 0.1 %, the specific surface area was lower than that of the sample without MEG. Excessive addition of GA can significantly increase powder flowability and insufficient stress events for effective particle size reduction. Consequently, this results in lower grindability due to incomplete grinding and potential negative impacts on classifier performance [49,72].

3.2. ICP-OES results

Fig. 5**(a and b)** illustrates the amount of Ca and Si ions released from the samples. In the O100 sample, the release of Ca ions was significantly high. This is likely due to the high Ca ions content in OPC. Meanwhile, samples with WG addition revealed interesting behaviors. In the case of the WG-OPC-0 % sample, a small amount of Ca ions was leached. Among the MEG-containing samples, as the MEG dosage increased, the initial release of Ca ions decreased, a trend that was particularly pronounced in the first 30 min. Furthermore, as the stirring time extended, the amount of Ca ions released from MEG-containing samples became nearly equivalent to that of the O100 sample. These findings suggest that the addition of WG led to less active C_2S and C_3S reactions, likely due to the reduced OPC content. Interestingly, the MEG-containing samples exhibited enhanced dissolution of C_2S and C_3S phases. This behavior is attributed to the mechanochemical effects of MEG on particle surfaces and dispersion. A more detailed discussion of this interpretation is provided later.

As expected, for Si ions, the inclusion of WG resulted in a substantial release of Si ions. In the MEG-containing samples, the amount of Si ions released increased with higher MEG dosages. It is worth emphasizing that despite the lower grindability of the WG-OPC-0.1 % sample, it exhibited a greater release of Si ions. However, this trend was not evident in samples stirred for 4 h. This suggests that during this period, a significant portion of the Si ions participated in hydration reactions, indicating substantial pozzolanic reactions between WG and CH phases [73,74]. In contrast, the WG-OPC-0.02 % and WG-OPC-0.05 % samples displayed lower Si ion release at the early stages. This could indicate either a significant consumption of Si ions in pozzolanic reactions before the 30-minute mark or inherently lower ion release. To investigate this further, the PONKCS method was employed for a quantitative analysis of WG and C-S-H contents, the results of which are detailed later in the discussion.

3.3. Calorimetric results

Fig. 6**(a and b)** illustrates the effects of MEG on the early hydration behavior of WG-OPC. A similar pattern was observed across all

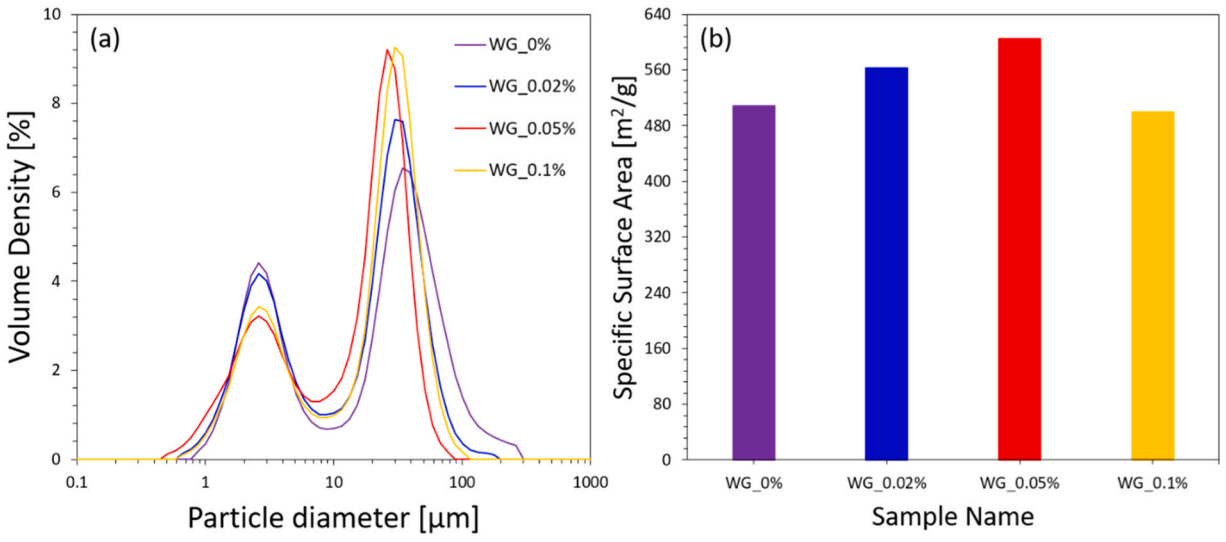

Fig. 4. Particle size distributions (a) and specific surface area (b) of WG with MEG application.

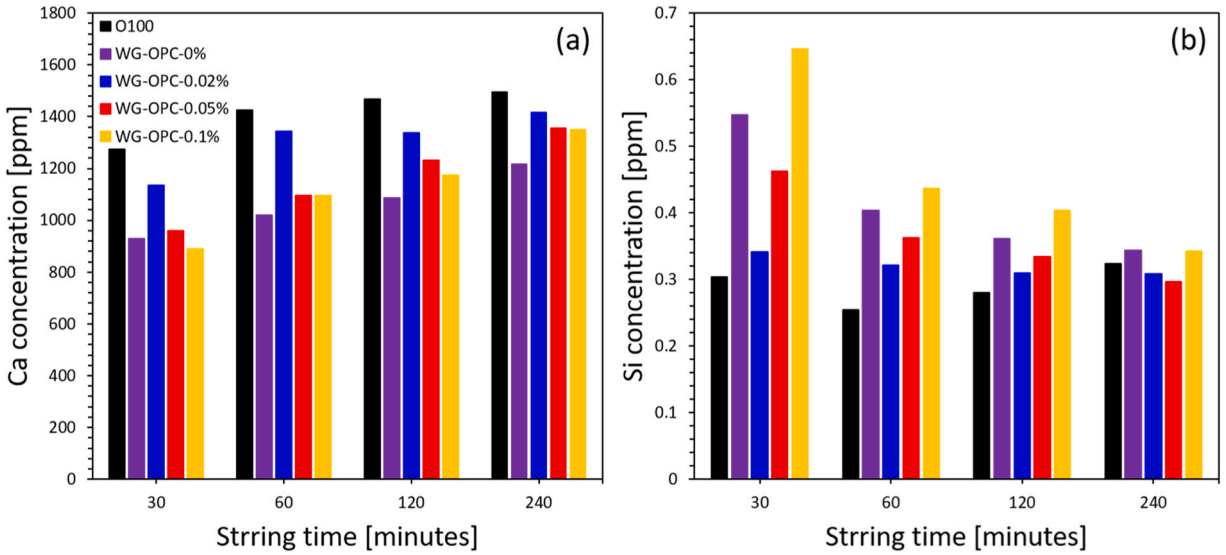

Fig. 5. ICP-OES results of samples.

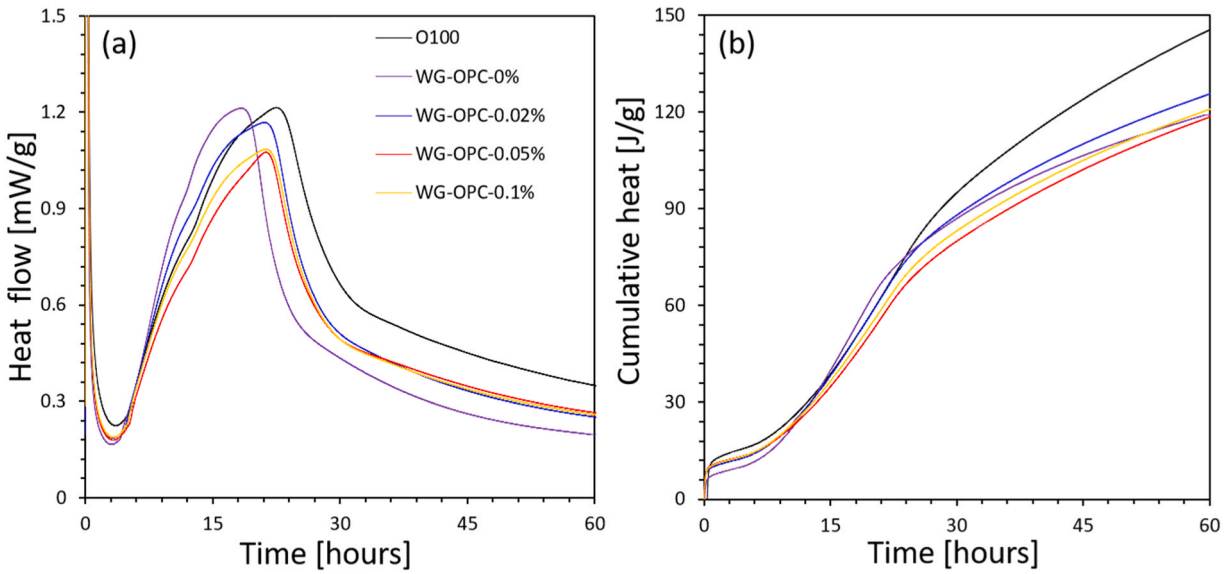

Fig. 6. Heat flow (a) and cumulative heat (b) of WG-OPC induced by MEG.

samples. Initially, a dissolution heat peak was detected, corresponding to the dissolution of binders into the water [75,76]. This was followed by an induction period lasting approximately 2–3 h, after which the main hydration peak, primarily associated with C_3S hydration, was observed [75–77]. Subsequently, an aluminate hydration peak, attributed to the hydration of C_3A and C_4AF, was identified [78–80]. That is, the heat release attributed to aluminate reactions was observed around 20–24 h, indicating that these reactions occurred appropriately after the silicate reactions. This suggests that the analyzed formulations exhibited a relatively optimal mix design.

However, some differences were noted between WG-OPC-0 % and O100 samples. In more detail, the addition of WG resulted in a reduction of dissolution heat, as well as a lower heat output during the induction period. This corresponds to results observed in previous reported [81]. Interestingly, the observation of the main hydration peak occurred slightly earlier in the WG-containing samples. This phenomenon can be attributed to the mechanochemical effect of WG-OPC. Furthermore, the duration of both the main hydration and aluminate hydration heat peaks was shorter overall. The hydration heat released after 30 h was significantly reduced.

In the samples containing MEG, notable differences were observed compared to the WG-OPC-0 % sample. Overall, the heat generated during the dissolution peak and the induction period increased. Furthermore, as the MEG dosage increased, the beginning of

the main hydration peak was delayed, approaching the timing observed in the O100 sample. However, the intensity of this peak was reduced. Furthermore, the hydration heats occurring after 30 h were higher than that of the WG-OPC-0 % sample. Consistent with previous findings, MEG generally delays the hydration reactions of OPC, and the delayed activation of WG hydration aligns with this behavior [82,83]. These early hydration characteristics could significantly influence the mechanical properties, not only in the early stages but also in the later stages. Moreover, the mineralogical properties of C-S-H, generated through the pozzolanic and silicate reactions (i.e., C_3S and C_2S), could vary, potentially leading to substantial differences in hydration heat. To investigate this further, this study quantitatively analyzed the pozzolanic activity of WG and the activity of its silicate phases. These findings will be discussed in greater detail later.

3.4. Compressive strength results

As shown in Fig. 7, the effects of MEG on the mechanical properties of WG-OPC are presented. To evaluate the strength activity index of WG as a pozzolan material, compressive strengths were measured at 1, 2, 7, and 28 days. Typically, pozzolan materials do not exhibit significant mechanical properties during the early stages, particularly within the first 1–2 days [25,45,84,85]. However, the obtained results revealed differing results for the 1–2 days compressive strengths. The WG-OPC-0 % sample showed a lower strength activity index than the O100 sample, and this trend became more pronounced at later stages. This implies that simply ground WG (without MEG) does not function effectively as a pozzolan material.

Interestingly, the addition of MEG resulted in distinctive trends. The samples with 0.02 % and 0.1 % MEG exhibited high early compressive strength but showed relatively inferior strength development at later stages, resulting in mechanical properties comparable to the O100 sample. This result differs somewhat from the commonly known fact that pozzolanic reactivity is typically activated at later stages [86,87]. However, the sample with 0.05 % MEG consistently exhibited compressive strengths that were comparable to or exceeded those of the O100 sample. In more detail, at 28 days, it achieved approximately 6.7 % higher compressive strength than the O100 sample, with a strength gain of approximately 38.2 % between 7 and 28 days. These results suggest that the mechanochemical effects of MEG on WG significantly enhance its hydration degree. In summary, this indicates that the pozzolan reactivity of WG can be finely tuned by adjusting the amount of MEG added.

3.5. CT results

Fig. 8**(a-e)** presents the original CT data, while Fig. 9 shows the cumulative porosity distributions of the samples cured for 28 days, as determined from CT measurements. In the case of the O100 sample, a total pore volume fraction of 2.09 % was observed, indicating a relatively low overall porosity. Interestingly, pores in the size range of 146.21–167.61 μm accounted for a significant 7.91 % of the total pore volume. For samples containing WG, the pore volume was generally higher. The total pore volume followed the order: WG-OPC-0 % > WG-OPC-0.1 % > WG-OPC-0.02 % > WG-OPC-0.05 %. Notably, the WG-OPC-0 % sample exhibited a greater number of large-diameter pores compared to the other samples. This trend showed a significant correlation with compressive strength, as an inverse relationship was observed between total pore volume and compressive strength. However, despite the O100 sample having a lower total pore volume than the WG-OPC-0.05 % sample, its mechanical properties were inferior, which contrasts with previously reported findings. This discrepancy may stem from differences in pore filling mechanisms resulting from the pozzolanic reaction of WG

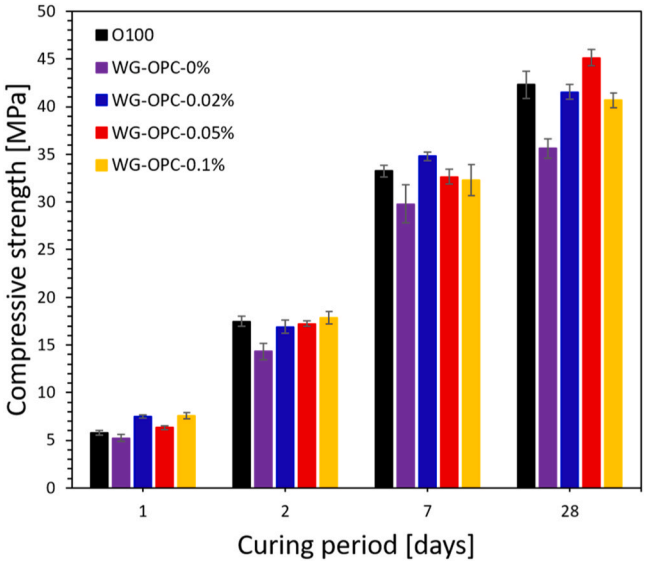

Fig. 7. Compressive strength results of WG-OPC with MEG.

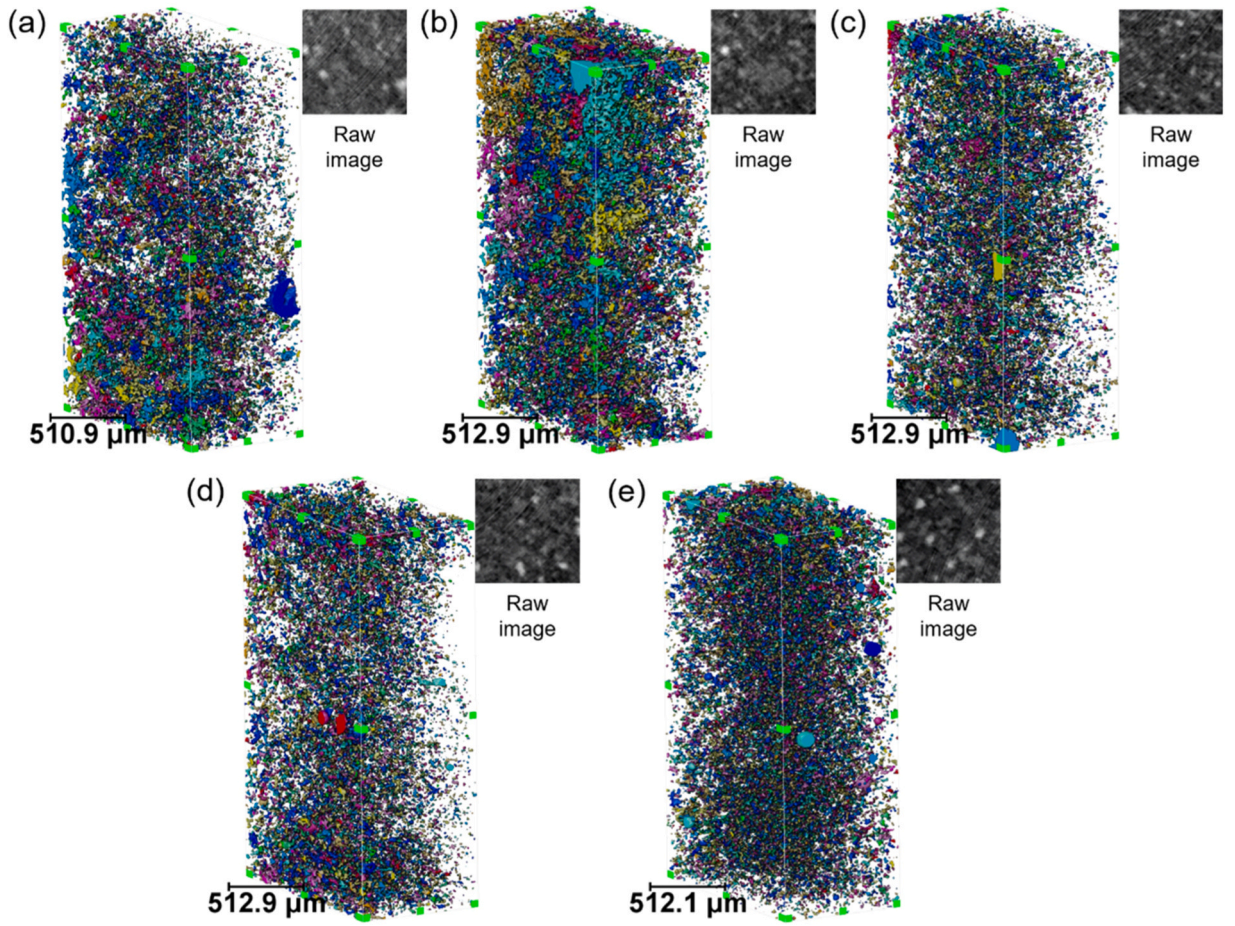

Fig. 8. Pore distribution and CT images of samples cured for 28 days: (a) O100, (b) WG-OPC-0 %, (c) WG-OPC-0.02 %, (d) WG-OPC-0.05 %, and (e) WG-OPC-0.1 %.

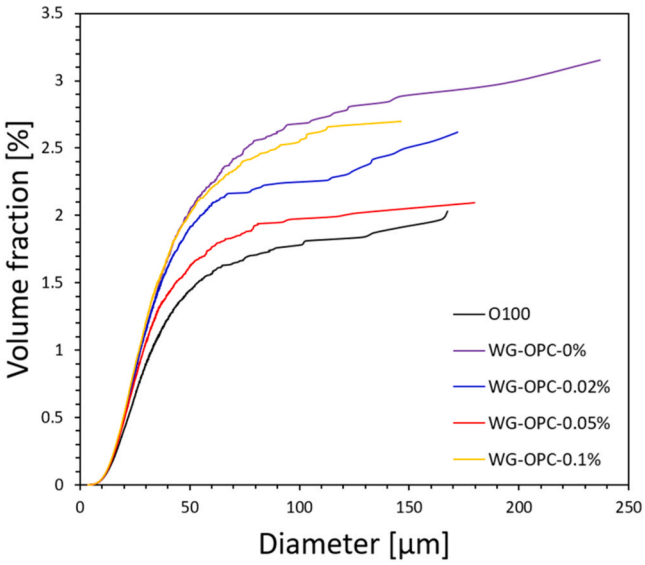

Fig. 9. Porosity properties analysis results of all samples cured for 28 days via CT measurement.

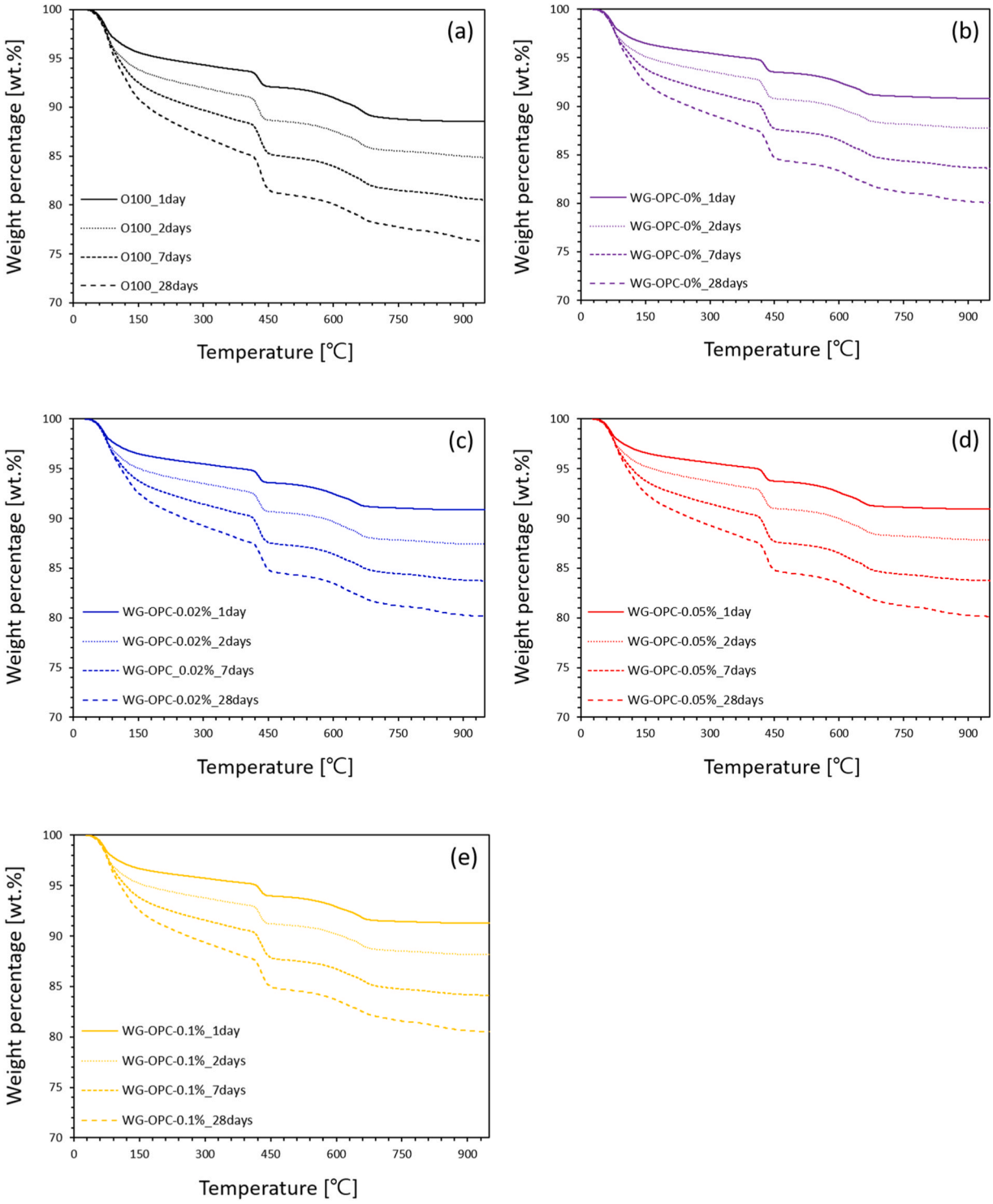

Fig. 10. TG results of (a) O100, (b) WG-OPC-0 %, (c) WG-OPC-0.02 %, (d) WG-OPC-0.05 %, and (e) WG-OPC-0.1 %.

and the hydration reaction of OPC. Therefore, further analysis of the hydration characteristics of WG-OPC composites is essential to clarify this phenomenon.

3.6. TGA results

Fig. 10**(a–e)** presents the TG measurement results according to curing duration and sample type. For all samples, the TG curves shifted downward as the curing duration increased. This is attributed to the increase in CBW within the hydration products formed as

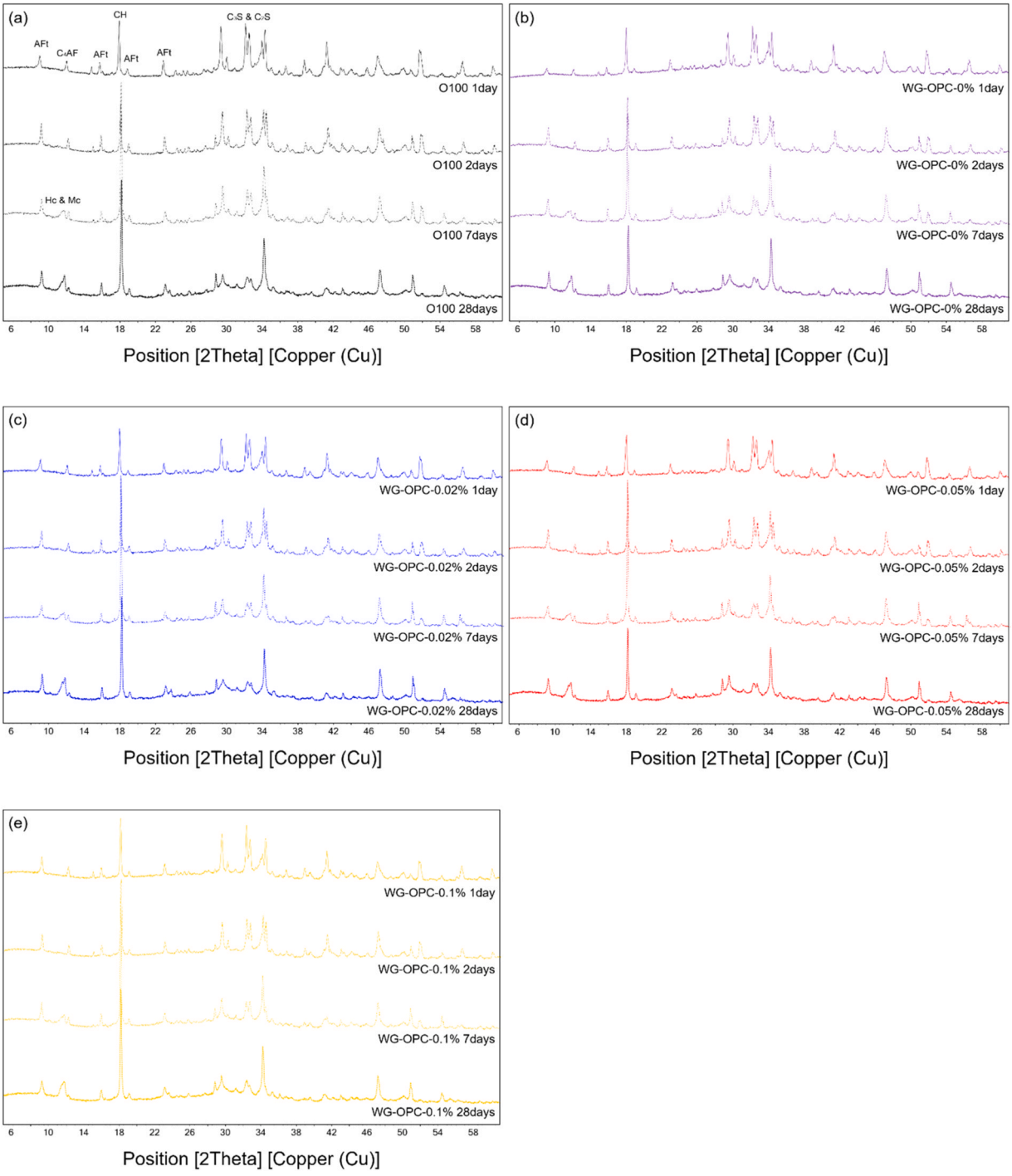

Fig. 11. XRD patterns: (a) O100, (b) WG-OPC-0 %, (c) WG-OPC-0.02 %, (d) WG-OPC-0.05 %, and (e) WG-OPC-0.1 %.

hydration progressed [10]. As expected, the samples containing WG exhibited a lower CBW content compared to the O100 sample. This indicates that OPC contributes a greater amount of CBW within its hydration products than WG.

Distinct weight loss regions were observed in the TG curves. The weight loss occurring between 400–500 °C and 600–800 °C corresponds to the thermal decomposition of calcium hydroxide (CH) and calcium carbonate (CC), respectively [62,88]. The amounts of both CH and CC increased with prolonged curing duration. In particular, CH is known to undergo a pozzolanic reaction with the amorphous SiO_2 in WG, rendering it a potential indicator of pozzolanic reactivity. However, due to CH carbonation and its continuous formation through OPC hydration, CH content alone cannot directly evaluate the pozzolanic reactivity of WG [89,90]. Therefore, in this study, the PONKCS method was introduced for a more precise analysis of pozzolan reactivity of WG, and detailed results will be discussed later.

3.7. XRD results

Fig. 11**(a-e)** presents the XRD patterns obtained for all curing durations investigated in this study. In the case of the O100 sample, the intensity of peaks corresponding to clinker minerals (C_3S, C_2S, C_3A, and C_4AF phases) decreased, as curing duration increased [46,

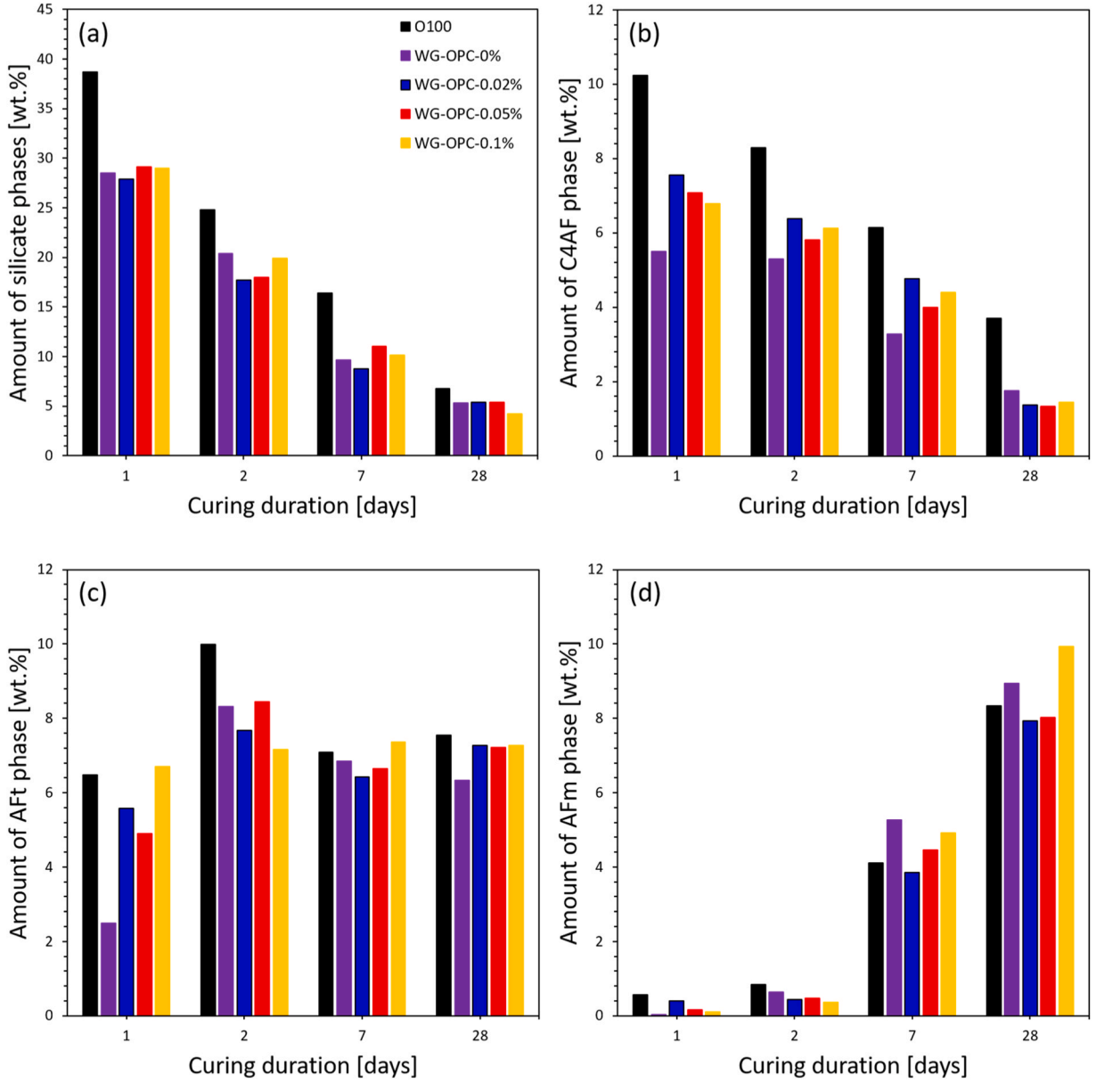

Fig. 12. Quantified amounts of phases: (a) silicate phases, (b) C_4AF, (c) AFt, and (d) AFm phases.

80,91]. Furthermore, AFt and CH hydration products were observed from 1 day, while hemicarboaluminate (Hc) and monocarboaluminate (Mc) phases appeared from 7 days. This hydration behavior is consistent with previous studies [92,93].

For the WG-OPC-0 % sample the hydration behavior was similar to that of O100 sample. Likewise, the WG-OPC-0.02 %, WG-OPC-0.05 %, and WG-OPC-0.1 % samples exhibited almost identical trends. However, special attention should be given to the CH. In some samples (i.e., samples cured for 7 days), a preferred orientation effect was observed in CH, rendering it difficult to determine its amount solely based on relative peak intensity [10,94,95]. Moreover, it is challenging to visually assess the extent of formation and consumption of the amorphous C-S-H and WG phases [62,96,97].

The QXRD analysis results for all samples are presented in Fig. 11**(a–e)**. Clinker minerals exhibited a continuous decrease, while hydration products (i.e., AFt, AFm, and CH phases) increased over time. In particular, the amount of C-S-H increased as the curing period progressed. Furthermore, in samples containing WG, a steady consumption of WG was observed. These trends varied significantly depending on the sample type, which could have a substantial impact on the mechanical properties of the composite [42,98,99]. A more detailed discussion of these effects will be provided in the discussion section.

4. Discussion

4.1. Impact of MEG on the OPC hydration in the WG-OPC system

Fig. 12**(a)** presents the amount of silicate phases for all samples and curing durations. In the case of the O100 sample, a relatively larger amount of unreacted silicate phases remained, which can be attributed to its higher OPC content. Nevertheless, by 28 days, all samples exhibited nearly the same residual amount of silicate phases. For the samples containing WG, significant differences were not observed, with most variations being within the range of 1–3 wt%. In particular, at 28 days, the remaining silicate phases were almost identical across all samples. The lack of change in silicate reactivity despite the addition of MEG differs somewhat from previously reported findings [10]. This discrepancy might be attributed to variations in the composite matrix environment, particularly in pH conditions.

Fig. 12**(b)** shows the quantity of the C_4AF. Similar to the silicate phases, the O100 sample retained a larger amount of C_4AF compared to the other samples. However, a different trend was observed in the WG-containing samples. That is, in the early stages, more C_4AF was consumed in the WG-OPC-0 % sample without MEG addition. In the absence of MEG, the sulfate sources appear to be partially adsorbed onto the C-S-H phase during the early stages, rather than contributing to the formation of AFt and AFm phases. In other words, in the WG-OPC-0 % sample, the formation of C-S-H was more pronounced, which may have led to a relatively higher amount of sulfate sources being partially adsorbed onto the C-S-H phase [100]. Nevertheless, by 28 days, the remaining amounts of C_4AF were nearly the same for all samples. Furthermore, Fig. 12**(c–d)** shows the formation of AFt and AFm. The formation of phases is closely related to the consumption of C_4AF and C_3A phases [44,47,101,102]. Overall, similar amounts of AFt and AFm were formed across all samples, with no significant differences observed. Based on these observations, the addition of WG with MEG did not have a substantial impact on silicate and aluminate reactions.

4.2. Activated pozzolan reactivity of WG-OPC due to MEG application

In this section, the silicate reactions and pozzolanic reaction of WG were discussed. As shown in Fig. 13**(a)**, the O100 sample exhibited a significant consumption of silicate phases at later stages, with the amount of consumed silicate phases being nearly

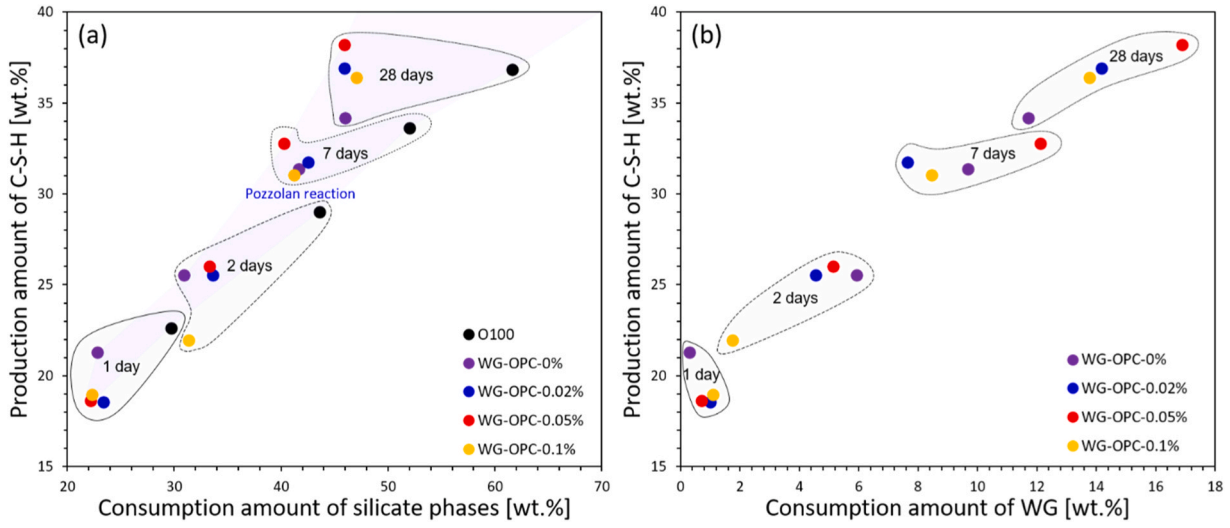

Fig. 13. Effect of MEG on (a) silicate and (b) WG hydration.

proportional to the formation of C-S-H. In contrast, the samples containing WG displayed a completely different trend. During the initial 1-day, the amount of consumed silicate phases was lower, and the formation of C-S-H was also relatively limited. However, except for the WG-OPC-0 % sample, the amount of C-S-H formed at 28 days was greater than that in the O100 sample. This trend was particularly pronounced in the WG-OPC-0.05 % sample. Therefore, these hydration behaviors indicate that the pozzolanic reactivity of WG contributed to the formation of the C-S-H [38,42,103].

As shown in Fig. 13**(b)**, the activation timing of the pozzolanic reaction of WG due to MEG addition can be identified. On the 1 day, the amount of WG consumed was nearly identical across all samples, regardless of the MEG dosage. However, a significant difference was observed between 1 and 2 days. In more detail, in the sample with 0.1 % MEG addition, only 0.66 wt% of WG was consumed, whereas in the other samples, WG consumption ranged from 3.54 to 5.62 wt%. Between 2 and 7 days, WG consumption was relatively higher in the samples with 0.05 % and 0.1 % MEG addition. From 7–28 days, a substantial amount of WG was consumed in all samples except for the WG-OPC-0 % sample. These results indicate that while MEG generally enhances the reactivity of WG during overall curing durations, excessive addition could reduce its effectiveness (i.e., In the WG-OPC-0.1 % sample during the initial 24 h). Over the total curing period of 28 days, the WG-OPC-0.05 % sample exhibited the highest WG consumption, with 67.52 % of the WG participating in the pozzolanic reaction. It is generally known that pozzolanic materials exhibit increased reactivity at later stages [82,83]. However, the results of this study revealed a somewhat different trend, demonstrating that the reactivity of WG can be effectively controlled by incorporating a small amount of MEG.

4.3. Enhancement of mechanical characteristics of WG-OPC

Fig. 14 illustrates the correlation between the amount of C-S-H formed and the development of compressive strength. The O100 sample and the WG-OPC-0 % sample exhibited a nearly identical trend in terms of the amount of C-S-H formed and the rate of compressive strength development. However, the overall compressive strength of the WG-OPC-0 % sample was lower. This can be attributed to the poor reactivity of simply ground WG (without MEG), as compared to that of OPC [42].

In contrast, the samples containing MEG exhibited a completely different trend. Despite the lower amount of C-S-H formation in the early stages, their initial compressive strengths were comparable. This phenomenon is likely due to the mechanochemical effects and packing density degree induced by MEG. In more detail, the pre-addition of MEG before WG grinding could have improved its grindability. MEG could have been uniformly adsorbed onto the WG particle surfaces [57,104] . Moreover, the particle size distribution of WG ensures an optimal packing density, which can refine porosity properties within the composite and consequently enhance its mechanical properties [105,106]. As a result of these effects, when 0.05 % MEG was added, the compressive strength surpassed that of the O100 sample. These effects were evident up to the first 2 days. However, after 7 days, the correlation between C-S-H formation and compressive strength development became nearly identical to that of the O100 sample. Furthermore, conclusions can be drawn regarding the potential occurrence of ASR. It is generally accepted that the addition of WG powder does not induce ASR. Since MEG itself does not directly alter the alkali concentration in the pore solution, its use, even though it enhances the pozzolanic reactivity of WG, is unlikely to significantly influence ASR formation [107]. This suggests that the ASR-related effects associated with MEG addition are relatively minor.

4.4. Mechanistic analysis of MEG-modified WG reactivity

This section explores the mechanistic basis for the enhancement in pozzolanic activity and composite performance achieved by MEG modification of WG. The adsorption of MEG on WG surfaces during grinding likely alters the surface properties of the glass particles. This is supported by the improved grindability observed at optimal dosages (i.e., 0.05 %), leading to increased specific surface area and finer particle size. MEG molecules, rich in hydroxyl groups, might physically adsorb onto the amorphous SiO_2 surfaces of WG, reducing agglomeration and promoting a more homogeneous dispersion. Such surface modification is hypothesized to enhance the dissolution kinetics of silica species during hydration, thereby facilitating more efficient reaction with calcium hydroxide to form C–S–H.

The influence of MEG dosage on WG performance exhibits a non-linear behavior. As shown in the pozzolanic activity results (Fig. 13), 0.05 % MEG addition resulted in the highest WG consumption and C–S–H formation. Lower dosage (0.02 %) enhanced early hydration but showed limited long-term gains, while higher dosage (0.1 %) delayed initial dissolution and reactivity due to potential saturation or steric hindrance effects. This implies a threshold beyond which MEG coverage on WG might hinder rather than promote reactivity. The balance between increased surface activation and potential hydration retardation must thus be carefully optimized.

Furthermore, the mechanochemical behavior of MEG in this system plays a dual role. First, as a GA, MEG improves WG grindability and dispersion, thereby enhancing packing density and early mechanical strength. Second, as a chemical modulator, MEG delays the hydration of OPC components, which allows for a more synchronized activation of WG's pozzolanic reactivity. The delayed onset of silicate hydration, coupled with increased ionic availability of WG (Ca^{2+}, Si^{4+}), supports the hypothesis that MEG fosters an environment conducive to gradual and sustained C–S–H growth. In this mechanism, MEG adsorbs onto WG during grinding, improving fineness and reducing agglomeration. Upon hydration, this modified WG surface releases Si^{4+} ions more readily, promoting pozzolanic reactions with $Ca(OH)_2$ (Fig. 15**(a and b)**). That is, MEG delays OPC hydration, providing a window for WG reactivity to manifest more fully. Consequently, the synergy between physical grinding enhancement and chemical modulation culminates in improved microstructure and strength performance of the WG-OPC composite.

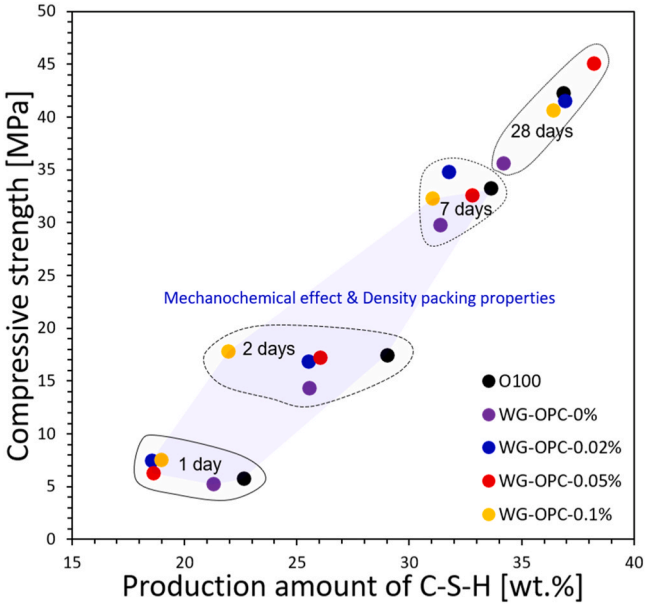

Fig. 14. Relationship between quantified amount of C-S-H and compressive strength.

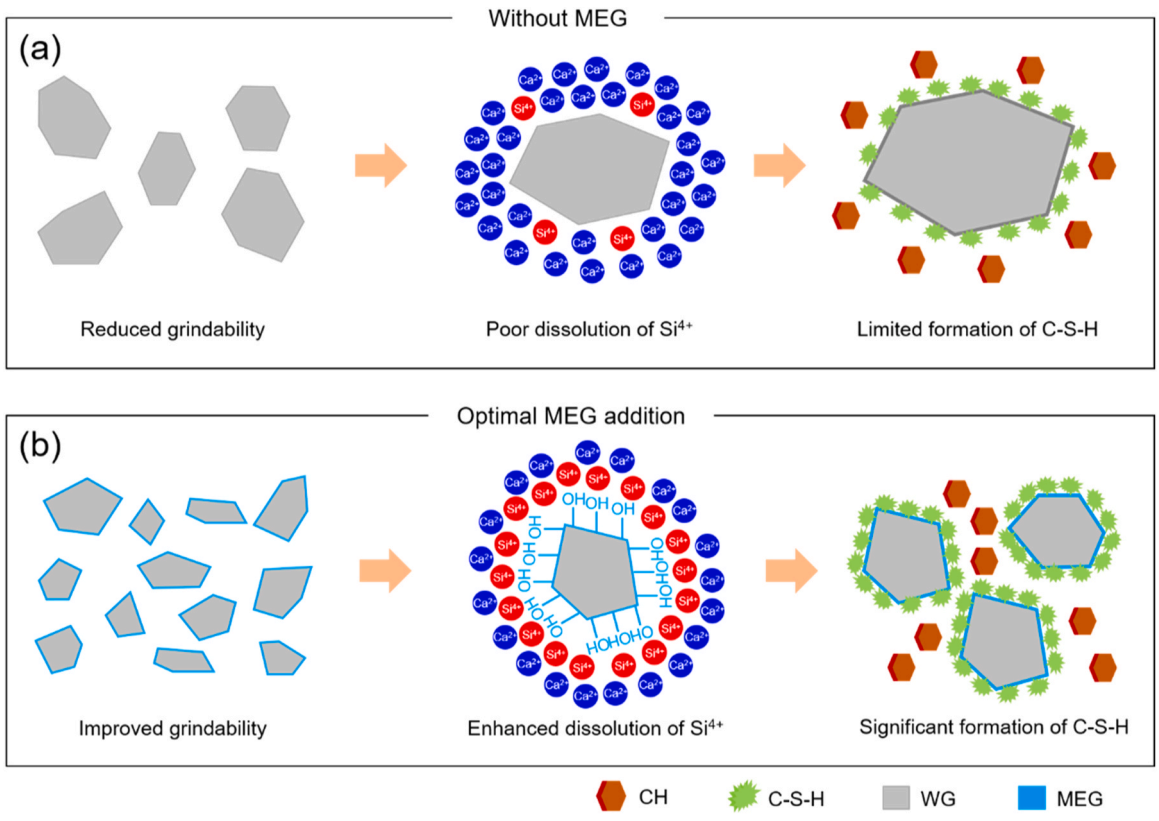

Fig. 15. Conceptual model of MEG-modified WG reactivity mechanism: (a) Sample without MEG addition, and (b) sample with optimal MEG dosage.

5. Conclusions

In this study, the impacts of four different dosages (i.e., 0, 0.02, 0.05, and 0.1 %) of MEG on the hydration and mechanical behaviors of WG-OPC composite were investigated. The time dependent hydration properties were analyzed using TGA, XRD, and isothermal calorimetry methods. Furthermore, the porosity characteristics were also analyzed using μ-CT. The key findings of this study are as follows:

1. The grindability of WG was significantly enhanced by adding MEG, with 0.05 % identified as the optimal dosage for maximizing grinding performance and pozzolanic reactivity.
2. At 0.05 % MEG, WG–OPC composites showed the highest WG consumption, greatest C-S-H formation, and notable reduction in total porosity, leading to improved mechanical properties.
3. Untreated WG exhibited limited pozzolanic activity, resulting in inferior mechanical performance at later stages.
4. Hydration behavior of OPC remained largely unchanged by MEG or WG additions; however, WG's pozzolanic reactivity strongly depended on MEG dosage.
5. Low to moderate MEG dosages (0.02 %–0.05 %) enhanced WG reactivity at both early and late stages, while higher dosage (0.1 %) delayed early reactivity but increased later-stage consumption.

These findings demonstrate that minimal MEG addition effectively improves WG's pozzolanic performance, offering a promising chemical grinding strategy to optimize WG as a supplementary cementitious material for sustainable cement composites. This study utilized a lab-scale ball mill to prepare WG-OPC composites. However, in practical applications, WG is typically ground using industrial-scale ball mills with much larger capacity. Therefore, one limitation of this study is that the lab-scale grinding conditions may not fully replicate real-world processing. Future research should focus on scaling up the process to validate the effectiveness of MEG as a grinding aid for WG under industrial conditions.

CRediT authorship contribution statement

Juhyuk Moon: Writing – review & editing, Validation, Supervision, Project administration, Funding acquisition, Conceptualization. **Chi Sun Poon:** Writing – review & editing, Validation, Supervision, Methodology, Conceptualization. **Jingwei Yang:** Investigation, Formal analysis, Data curation. **Jian-Xin Lu:** Validation, Methodology, Conceptualization. **Namgyu Park:** Investigation, Formal analysis, Data curation. **Ahyeon Lim:** Investigation, Formal analysis, Data curation. **Hyunuk Kang:** Writing – original draft, Visualization, Methodology, Investigation, Formal analysis, Data curation, Conceptualization.

Declaration of Competing Interest

The authors declare that they have no known competing financial interests or personal relationships that could have appeared to influence the work reported in this paper.

Acknowledgments

This work was supported by the Industrial Strategic Technology Development Program–Development of Manufacturing Technology of Hardened Cement with Carbonation Curing (RS-2022–00155662, Development of manufacturing and application technology of 1000 ton/year class hardened cement with carbonation curing) funded by the Ministry of Trade, Industry & Energy (MOTIE, Korea). The Institute of Engineering Research in Seoul National University provided research facilities for this work.

Appendix A. Supporting information

Supplementary data associated with this article can be found in the online version at doi:10.1016/j.cscm.2025.e05336.

Data availability

Data will be made available on request.

References

[1] H.J. Kang, B. Tamang, J. Jin, S. Lee, Y. Kim, Performance evaluation of ultrafine cement as a grout for reservoir impermeability improvement, Acta Geotech. 18 (2) (2023) 1057–1072.
[2] S.A. Miller, G. Habert, R.J. Myers, J.T. Harvey, Achieving net zero greenhouse gas emissions in the cement industry via value chain mitigation strategies, One Earth 4 (10) (2021) 1398–1411.
[3] K.L. Scrivener, V.M. John, E.M. Gartner, Eco-efficient cements: potential economically viable solutions for a low-CO2 cement-based materials industry, Cem. Concr. Res. 114 (2018) 2–26.

[4] E. De Lena, M. Spinelli, M. Gatti, R. Scaccabarozzi, S. Campanari, S. Consonni, G. Cinti, M.C. Romano, Techno-economic analysis of calcium looping processes for low CO2 emission cement plants, Int. J. Greenh. Gas. Control 82 (2019) 244–260.
[5] T.A. Santos, M.S. Cilla, Use of asbestos cement tile waste (ACW) as mineralizer in the production of portland cement with low CO2 emission and lower energy consumption, J. Clean. Prod. 335 (2022) 130061.
[6] S.A. Miller, V.M. John, S.A. Pacca, A. Horvath, Carbon dioxide reduction potential in the global cement industry by 2050, Cem. Concr. Res. 114 (2018) 115–124.
[7] J.A. Olsson, S.A. Miller, M.G. Alexander, Near-term pathways for decarbonizing global concrete production, Nat. Commun. 14 (1) (2023) 4574.
[8] D. Das, P.K. Rout, A review of coal Fly ash utilization to save the environment, Water Air Soil Pollut. 234 (2) (2023) 128.
[9] L. Xu, J. Wang, K. Li, T. Hao, Z. Li, L. Li, B. Ran, H. Du, New insights on dehydration at elevated temperature and rehydration of GGBS blended cement, Cem. Concr. Compos. 139 (2023) 105068.
[10] H. Kang, J. Yang, J. Pae, S. Kim, S.-H. Kang, J. Moon, The impact of mono-ethylene glycol on ordinary portland cement: exploring grindability, workability, hydration, and mechanical properties, Cem. Concr. Compos. 154 (2024) 105789.
[11] N. Nisar, I. Rahman, S. Paruthi, A.H. Khan, E. Sabi, A. Alyaseen, Enhancing concrete properties with nano-SiO2 and nano-TiO2: a review, J. Struct. Integr. Maint. 10 (2) (2025) 2496613.
[12] Y. Li, T. Li, Y. Li, S. Zhang, X. Chen, H. Yan, X. Liu, W. Ni, Reactivation and utilization study of melting furnace slag generated from co-processing MSW incineration Fly ash, Green Energy Resour. 1 (3) (2023) 100035.
[13] H. Feng, X. Xin, A. Guo, Z. Yu, Q. Shao, M.N. Sheikh, Z. Sun, Effect of mix proportion parameters on chloride erosion resistance of Fly ash/slag-based engineered geopolymer composites, J. Clean. Prod. 438 (2024) 140785.
[14] J.M. Etcheverry, Y.A. Villagran-Zaccardi, P. Van den Heede, N. De Belie, Efficient use of Low-Calcium Fly ash to reach replacement levels beyond 50% portland cement with curing at room temperature, J. Build. Eng. (2025) 113435.
[15] H. Wang, G. Tan, P. Lin, F. Gu, J. Zhang, Performance evaluation of geopolymer grout materials derived from high-volume circulating fluidized bed Fly ash and ground granulated blast furnace slag, Constr. Build. Mater. 474 (2025) 141082.
[16] A. Badkul, R. Paswan, S. Singh, J. Tegar, A comprehensive study on the performance of alkali activated Fly ash/GGBFS geopolymer concrete pavement, Road. Mater. Pavement Des. 23 (8) (2022) 1815–1835.
[17] A. Varshney, P. Dahiya, A. Sharma, R. Pandey, S. Mohan, Fly ash application in soil for sustainable agriculture: an Indian overview, Energy Ecol. Environ. 7 (4) (2022) 340–357.
[18] Y. Jani, W. Hogland, Waste glass in the production of cement and concrete–A review, J. Environ. Chem. Eng. 2 (3) (2014) 1767–1775.
[19] E. Harrison, A. Berenjian, M. Seifan, Recycling of waste glass as aggregate in cement-based materials, Environ. Sci. Ecotechnol. 4 (2020) 100064.
[20] A. Mehta, D.K. Ashish, Silica fume and waste glass in cement concrete production: a review, J. Build. Eng. 29 (2020) 100888.
[21] K. Sobolev, P. Türker, S. Soboleva, G. Iscioglu, Utilization of waste glass in ECO-cement: strength properties and microstructural observations, Waste Manag. 27 (7) (2007) 971–976.
[22] B. Qin, Z. Yao, K. Deng, J. Ruan, Z. Xu, Analysis of contaminants and their formation mechanism in the desiccation-dissociation process of organic impurity of waste glass, J. Hazard. Mater. 416 (2021) 125881.
[23] T. Gallucci, G. Lagioia, P. Piccinno, A. Lacalamita, A. Pontrandolfo, A. Paiano, Environmental performance scenarios in the production of hollow glass containers for food packaging: an LCA approach, Int. J. Life Cycle Assess. 26 (2021) 785–798.
[24] R. Deng, N.L. Chang, Z. Ouyang, C.M. Chong, A techno-economic review of silicon photovoltaic module recycling, Renew. Sustain. Energy Rev. 109 (2019) 532–550.
[25] A. Mohajerani, J. Vajna, T.H.H. Cheung, H. Kurmus, A. Arulrajah, S. Horpibulsuk, Practical recycling applications of crushed waste glass in construction materials: a review, Constr. Build. Mater. 156 (2017) 443–467.
[26] D. Patel, R. Tiwari, R. Shrivastava, R. Yadav, Effective utilization of waste glass powder as the substitution of cement in making paste and mortar, Constr. Build. Mater. 199 (2019) 406–415.
[27] K. Afshinnia, P.R. Rangaraju, Influence of fineness of ground recycled glass on mitigation of alkali–silica reaction in mortars, Constr. Build. Mater. 81 (2015) 257–267.
[28] A.M. Rashad, Recycled waste glass as fine aggregate replacement in cementitious materials based on portland cement, Constr. Build. Mater. 72 (2014) 340–357.
[29] I.S. Kim, S.Y. Choi, E.I. Yang, Evaluation of durability of concrete substituted heavyweight waste glass as fine aggregate, Constr. Build. Mater. 184 (2018) 269–277.
[30] S.B. Park, B.C. Lee, J.H. Kim, Studies on mechanical properties of concrete containing waste glass aggregate, Cem. Concr. Res. 34 (12) (2004) 2181–2189.
[31] F. Rajabipour, H. Maraghechi, G. Fischer, Investigating the alkali-silica reaction of recycled glass aggregates in concrete materials, J. Mater. Civ. Eng. 22 (12) (2010) 1201–1208.
[32] H. Maraghechi, G. Fischer, F. Rajabipour, The role of residual cracks on alkali silica reactivity of recycled glass aggregates, Cem. Concr. Compos. 34 (1) (2012) 41–47.
[33] L. Sun, X. Zhu, M. Kim, G. Zi, Alkali-silica reaction and strength of concrete with pretreated glass particles as fine aggregates, Constr. Build. Mater. 271 (2021) 121809.
[34] S. Yang, X. Dong, X. Zhao, J.-X. Lu, H. Cui, C.S. Poon, High value-added utilization of waste glass powder and steel slag for a novel zero-clinker cement: coactivation mechanism and environmental impact, Constr. Build. Mater. 474 (2025) 141032.
[35] X. Zhang, H. Zhao, Z. Tao, W. Li, Performance of sustainable cementitious mortar incorporating hybrid waste glass powder and steel slag, Constr. Build. Mater. 472 (2025) 140928.
[36] F. Ren, X. Zhang, Y. Ye, Q. Wang, J. Xu, Enhancement effect of waste glass powder on the compressive fatigue behavior of concrete, Constr. Build. Mater. 489 (2025) 142215.
[37] B. Jia, L. Peng, Y. Zhao, Recycling waste glass powder in lightweight aggregate concrete: towards lightweight, sustainable and durable marine engineering structures, Constr. Build. Mater. 472 (2025) 140690.
[38] E.T. Bueno, J.M. Paris, K.A. Clavier, C. Spreadbury, C.C. Ferraro, T.G. Townsend, A review of ground waste glass as a supplementary cementitious material: a focus on alkali-silica reaction, J. Clean. Prod. 257 (2020) 120180.
[39] G. Ke, W. Li, R. Li, Y. Li, G. Wang, Mitigation effect of waste glass powders on alkali–silica reaction (ASR) expansion in cementitious composite, Int. J. Concr. Struct. Mater. 12 (2018) 1–14.
[40] Y. Cai, D. Xuan, C.S. Poon, Effects of nano-SiO2 and glass powder on mitigating alkali-silica reaction of cement glass mortars, Constr. Build. Mater. 201 (2019) 295–302.
[41] R. Idir, M. Cyr, A. Tagnit-Hamou, Pozzolanic properties of fine and coarse color-mixed glass cullet, Cem. Concr. Compos. 33 (1) (2011) 19–29.
[42] L. Federico, S. Chidiac, Waste glass as a supplementary cementitious material in concrete–critical review of treatment methods, Cem. Concr. Compos. 31 (8) (2009) 606–610.
[43] A. Khmiri, M. Chaabouni, B. Samet, Chemical behaviour of ground waste glass when used as partial cement replacement in mortars, Constr. Build. Mater. 44 (2013) 74–80.
[44] H. Kang, S. Kim, Y. Lee, S. Jung, J. Moon, Mechanochemical effect of alkanolamines on the C4AF: crystal structure, hydration behavior, and strength enhancement, Cem. Concr. Compos. 145 (2024) 105326.
[45] H. Kang, J. Yang, S. Kim, A. Lim, J. Moon, Mechanochemical activation for transforming bottom ash to reactive supplementary cementitious material, Constr. Build. Mater. 411 (2024) 134523.
[46] H. Kang, S.-H. Kang, J. Moon, A comparative investigation of hydration reaction of portland cement with the use of alkanolamine as a chemical admixture or grinding agent under laboratory condition, J. Build. Eng. 88 (2024) 109214.

[47] H. Kang, J. Lee, J. Yang, J. Moon, Impact of triisopropanolamine on surface composition, crystallographic variation, and thermal behavior of C3A polymorphs, Mater. Struct. 57 (4) (2024) 1–19.
[48] H. Kang, S. Jung, J. Jung, J. Park, J.-B. Park, J. Moon, Investigation of the effect of diethanol isopropanolamine on ferrite phase, J. Sustain. Cem. Based Mater. 12 (12) (2023) 1604–1616.
[49] W. Li, S. Ma, Y. Hu, X. Shen, The mechanochemical process and properties of portland cement with the addition of new alkanolamines, Powder Technol. 286 (2015) 750–756.
[50] X. Lu, Z. Ye, L. Zhang, P. Hou, X. Cheng, The influence of ethanol-diisopropanolamine on the hydration and mechanical properties of portland cement, Constr. Build. Mater. 135 (2017) 484–489.
[51] S. Yang, J. Wang, S. Cui, H. Liu, X. Wang, Impact of four kinds of alkanolamines on hydration of steel slag-blended cementitious materials, Constr. Build. Mater. 131 (2017) 655–666.
[52] F. Zunino, K. Scrivener, Assessing the effect of alkanolamine grinding aids in limestone calcined clay cements hydration, Constr. Build. Mater. 266 (2021) 121293.
[53] S. Ma, W. Li, S. Zhang, Y. Hu, X. Shen, Study on the hydration and microstructure of portland cement containing diethanol-isopropanolamine, Cem. Concr. Res. 67 (2015) 122–130.
[54] Z. Xu, W. Li, J. Sun, Y. Hu, K. Xu, S. Ma, X. Shen, Research on cement hydration and hardening with different alkanolamines, Constr. Build. Mater. 141 (2017) 296–306.
[55] I. Teoreanu, G. Guslicov, Mechanisms and effects of additives from the dihydroxy-compound class on portland cement grinding, Cem. Concr. Res. 29 (1) (1999) 9–15.
[56] J.J. Assaad, S.E. Asseily, J. Harb, Effect of specific energy consumption on fineness of portland cement incorporating amine or glycol-based grinding aids, Mater. Struct. 42 (2009) 1077–1087.
[57] S. Sohoni, R. Sridhar, G. Mandal, The effect of grinding aids on the fine grinding of limestone, quartz and portland cement clinker, Powder Technol. 67 (3) (1991) 277–286.
[58] F. Hashem, E. Hekal, M. Wahab, The influence of triethanol amine and ethylene glycol on the grindability, setting and hydration characteristics of portland cement, Petrol. Chem. 4 (2019) 81–88.
[59] Y. Zhou, C.A. Orozco, E. Duque-Redondo, H. Manzano, G. Geng, P. Feng, P.J. Monteiro, C. Miao, Modification of poly (ethylene glycol) on the microstructure and mechanical properties of calcium silicate hydrates, Cem. Concr. Res. 115 (2019) 20–30.
[60] W. Guan, F. Ji, Q. Chen, P. Yan, L. Pei, Synthesis and enhanced phosphate recovery property of porous calcium silicate hydrate using polyethyleneglycol as pore-generation agent, Materials 6 (7) (2013) 2846–2861.
[61] F. Caruso, S. Mantellato, M. Palacios, R.J. Flatt, ICP-OES method for the characterization of cement pore solutions and their modification by polycarboxylate-based superplasticizers, Cem. Concr. Res. 91 (2017) 52–60.
[62] H. Kang, J. Moon, Secondary curing effect on the hydration of ultra-high performance concrete, Constr. Build. Mater. 298 (2021) 123874.
[63] Y. Jeong, C.W. Hargis, H. Kang, S.-C. Chun, J. Moon, The effect of elevated curing temperatures on high ye'elimite calcium sulfoaluminate cement mortars, Materials 12 (7) (2019) 1072.
[64] S. Maheswaran, S. Kalaiselvam, S.S. Karthikeyan, C. Kokila, G. Palani, β-Belite cements (β-dicalcium silicate) obtained from calcined lime sludge and silica fume, Cem. Concr. Compos. 66 (2016) 57–65.
[65] Y. Jeong, S.-H. Kang, M.O. Kim, J. Moon, Acceleration of cement hydration from supplementary cementitious materials: performance comparison between silica fume and hydrophobic silica, Cem. Concr. Compos. 112 (2020) 103688.
[66] L. Finger, D. Cox, A. Jephcoat, A correction for powder diffraction peak asymmetry due to axial divergence, J. Appl. Crystallogr. 27 (6) (1994) 892–900.
[67] A. Gualtieri, P. Norby, J. Hanson, J. Hriljac, Rietveld refinement using synchrotron X-ray powder diffraction data collected in transmission geometry using an imaging-plate detector: application to standard m-ZrO2, J. Appl. Crystallogr. 29 (6) (1996) 707–713.
[68] X. Li, R. Snellings, K.L. Scrivener, Quantification of amorphous siliceous Fly ash in hydrated blended cement pastes by X-ray powder diffraction, J. Appl. Crystallogr. 52 (6) (2019) 1358–1370.
[69] R. Snellings, A. Salze, K. Scrivener, Use of X-ray diffraction to quantify amorphous supplementary cementitious materials in anhydrous and hydrated blended cements, Cem. Concr. Res. 64 (2014) 89–98.
[70] S. Bergold, F. Goetz-Neunhoeffer, J. Neubauer, Quantitative analysis of C–S–H in hydrating alite pastes by in-situ XRD, Cem. Concr. Res. 53 (2013) 119–126.
[71] N. Otsu, A threshold selection method from gray-level histograms, IEEE Trans. Syst. Man Cybern. 9 (1) (1979) 62–66.
[72] P. Prziwara, A. Kwade, Grinding aid additives for dry fine grinding processes–Part II: continuous and industrial grinding, Powder Technol. 394 (2021) 207–213.
[73] A. Bouchikhi, M. Benzerzour, N.-E. Abriak, W. Maherzi, Y. Mamindy-Pajany, Study of the impact of waste glasses types on pozzolanic activity of cementitious matrix, Constr. Build. Mater. 197 (2019) 626–640.
[74] A. Hajimohammadi, J.S. van Deventer, Dissolution behaviour of source materials for synthesis of geopolymer binders: a kinetic approach, Int. J. Miner. Process. 153 (2016) 80–86.
[75] D. Jansen, F. Goetz-Neunhoeffer, B. Lothenbach, J. Neubauer, The early hydration of ordinary portland cement (OPC): an approach comparing measured heat flow with calculated heat flow from QXRD, Cem. Concr. Res. 42 (1) (2012) 134–138.
[76] D. Jansen, F. Goetz-Neunhoeffer, C. Stabler, J. Neubauer, A remastered external standard method applied to the quantification of early OPC hydration, Cem. Concr. Res. 41 (6) (2011) 602–608.
[77] I. Kirchberger, F. Goetz-Neunhoeffer, J. Neubauer, Enhancing the aluminate reaction during OPC hydration by combining increased sulfate content, triethanolamine and tartaric acid, Cem. Concr. Res. 170 (2023) 107188.
[78] R.J. Myers, G. Geng, J. Li, E.D. Rodríguez, J. Ha, P. Kidkhunthod, G. Sposito, L.N. Lammers, A.P. Kirchheim, P.J. Monteiro, Role of adsorption phenomena in cubic tricalcium aluminate dissolution, Langmuir 33 (1) (2017) 45–55.
[79] F. Zunino, K. Scrivener, Factors influencing the sulfate balance in pure phase C3S/C3A systems, Cem. Concr. Res. 133 (2020) 106085.
[80] S. Jung, H. Kang, S.-H. Kang, J. Moon, Alkanolamine-based chemically enhanced hydration reaction of ordinary portland cement, Constr. Build. Mater. 409 (2023) 134045.
[81] J.-x Lu, Z.-h Duan, C.S. Poon, Fresh properties of cement pastes or mortars incorporating waste glass powder and cullet, Constr. Build. Mater. 131 (2017) 793–799.
[82] C.B. Sawyer, J.S. Reed, Adsorption of hydroxypropyl methyl cellulose in an aqueous system containing multicomponent oxide particles, J. Am. Ceram. Soc. 84 (6) (2001) 1241–1249.
[83] L. Zhao, P. Feng, L. Shao, S. Ye, X. Liu, Using viscosity modifying admixture to reduce diffusion in cement-based materials: effect of molecular mass, Constr. Build. Mater. 290 (2021) 123207.
[84] H. Kang, A. Lim, J. Moon, Utilization of low reactive bottom ash in cement formulation through Na2CO3 triggered pozzolanic reaction, Constr. Build. Mater. 408 (2023) 133688.
[85] Y. Shao, T. Lefort, S. Moras, D. Rodriguez, Studies on concrete containing ground waste glass, Cem. Concr. Res. 30 (1) (2000) 91–100.
[86] F. Cassagnabère, G. Escadeillas, M. Mouret, Study of the reactivity of cement/metakaolin binders at early age for specific use in steam cured precast concrete, Constr. Build. Mater. 23 (2) (2009) 775–784.
[87] M. Carsana, M. Frassoni, L. Bertolini, Comparison of ground waste glass with other supplementary cementitious materials, Cem. Concr. Compos. 45 (2014) 39–45.
[88] S. Granger, A. Loukili, G. Pijaudier-Cabot, G. Chanvillard, Mechanical characterization of the self-healing effect of cracks in Ultra High Performance Concrete (UHPC), In:Proceedings Third International Conference on Construction Materials, Performance, Innovations and Structural Implications, ConMat, 2005, pp. 22-24.

[89] K. Wan, Q. Xu, Y. Wang, G. Pan, 3D spatial distribution of the calcium carbonate caused by carbonation of cement paste, Cem. Concr. Compos. 45 (2014) 255–263.
[90] S. Wang, Quantitative kinetics of pozzolanic reactions in coal/cofired biomass Fly ashes and calcium hydroxide (CH) mortars, Constr. Build. Mater. 51 (2014) 364–371.
[91] H. Kang, Y. Lee, J. Lee, J. Moon, Importance of amorphous content, surface energy, and preferred orientation on the accurate quantification of cement minerals in clinkers, J. Build. Eng. 66 (2023) 105887.
[92] S. Kim, J. Yang, J. Lee, C. sun Poon, J. Moon, Impact of triethanolamine on grinding and hydration performance of BOF steel slag blended cement, J. Build. Eng. (2025) 111858.
[93] J. Lee, A. Lim, H. Kang, D. Jeon, N. Lee, C. sun Poon, J. Moon, Understanding the effect of triethanolamine on grinding and hydration of blast furnace slag, focusing on the degrees of slag consumption and c (-A)-SH formation, Constr. Build. Mater. 458 (2025) 139693.
[94] R.J. Detwiler, P.J. Monteiro, H.-R. Wenk, Z. Zhong, Texture of calcium hydroxide near the cement paste-aggregate interface, Cem. Concr. Res. 18 (5) (1988) 823–829.
[95] V.S. Harutyunyan, E.S. Abovyan, P.J. Monteiro, V.P. Mkrtchyan, M.K. Balyan, A.P. Aivazyan, X-ray diffraction investigations of microstructure of calcium hydroxide crystallites in the interfacial transition zone of concrete, J. Am. Ceram. Soc. 86 (12) (2003) 2162–2166.
[96] J. Wang, H. Li, Z. Hu, Z. Li, J. Liu, Phase quantification analysis in cement-blended slag system with the PONKCS method, J. Sustain. Cem. Based Mater. 13 (9) (2024) 1390–1405.
[97] C. Naber, S. Stegmeyer, D. Jansen, F. Goetz-Neunhoeffer, J. Neubauer, The PONKCS method applied for time resolved XRD quantification of supplementary cementitious material reactivity in hydrating mixtures with ordinary portland cement, Constr. Build. Mater. 214 (2019) 449–457.
[98] C. Shi, Y. Wu, C. Riefler, H. Wang, Characteristics and pozzolanic reactivity of glass powders, Cem. Concr. Res. 35 (5) (2005) 987–993.
[99] N. Schwarz, H. Cam, N. Neithalath, Influence of a fine glass powder on the durability characteristics of concrete and its comparison to Fly ash, Cem. Concr. Compos. 30 (6) (2008) 486–496.
[100] F. Zunino, K. Scrivener, Microstructural developments of limestone calcined clay cement (LC3) pastes after long-term (3 years) hydration, Cem. Concr. Res. 153 (2022) 106693.
[101] H. Kang, Y. Lee, S. Jung, J. Moon, Enhanced hydration reaction of synthesized C4A0. 81F1. 19 with the use of different grinding agents, Mater. Struct. 57 (9) (2024) 1–18.
[102] S. Ye, P. Feng, J. Liu, Dissolution and early hydration of tetracalcium aluminoferrite (C4AF) in water and in aqueous sulfate solutions, Cem. Concr. Res. 186 (2024) 107676.
[103] Q. Li, H. Qiao, A. Li, G. Li, Performance of waste glass powder as a pozzolanic material in blended cement mortar, Constr. Build. Mater. 324 (2022) 126531.
[104] P.R. Nair, R. Paramasivam, Effect of grinding aids on the time-flow characteristics of the ground product from a batch ball mill, Powder Technol. 101 (1) (1999) 31–42.
[105] L. Li, A. Kwan, Packing density of concrete mix under dry and wet conditions, Powder Technol. 253 (2014) 514–521.
[106] X. Wang, R. Yu, Q. Song, Z. Shui, Z. Liu, S. Wu, D. Hou, Optimized design of ultra-high performance concrete (UHPC) with a high wet packing density, Cem. Concr. Res. 126 (2019) 105921.
[107] T. Yoshioka, T. Kameda, S. Imai, A. Okuwaki, Dechlorination of poly(vinyl chloride) using NaOH in ethylene glycol under atmospheric pressure, Polym. Degrad. Stab. 93 (6) (2008) 1138–1141.